Article:
Terzioglu, F. orcid.org/0000-0002-2639-2992, Rongong, J. and Lord, C. (2023) Motional phase maps for estimating the effectiveness of granular dampers. Mechanical Systems and Signal Processing, 188. 110038. ISSN 0888-3270

https://doi.org/10.1016/j.ymssp.2022.110038

Mechanical Systems and Signal Processing 188 (2023) 110038

Contents lists available at ScienceDirect

Mechanical Systems and Signal Processing

journal homepage: www.elsevier.com/locate/ymssp

Motional phase maps for estimating the effectiveness of granular dampers

Furkan Terzioglu *, Jem Athing Rongong, Charles Eric Lord

Department of Mechanical Engineering, University of Sheffield, Mappin Street, Sheffield S1 3JD, United Kingdom

ARTICLE INFO

Keywords:
Granular energy dissipation
Particle damper
Particle motion
Granular motion phase
Particle fluidisation
Bouncing bed

ABSTRACT

This paper evaluates simple but general links between the operating dynamic motional phases and the non-linear energy dissipation characteristics of granular dampers. The Discrete Element Method is used to simulate a typical granular medium consisting of spherical particles in a cylindrical enclosure subjected to harmonic vibrations aligned both parallel and perpendicular with gravity. A set of equivalent experiments is conducted to verify the numerical model. A wide range of excitation frequency and amplitude are considered, to obtain many different motional phases, along with particle size and volume fill ratio. Granular motional phase maps are produced over amplitude-frequency plane that defines where the various motion phases are present providing rich information for the effectiveness of granular dampers. Findings show that high granular damping effectiveness is found in two distinct zones: where collective collisions with the enclosure are optimised and where fluidisation without convection is maximised. The most significant factors affecting these high effectiveness zones are identified and can be used to provide guidance for those seeking to design granular dampers to reduce vibrations in structures.

1. Introduction

Granular damping is a particulate-based method for removing vibrational energy from mechanical systems. A granular damper typically consists of many relatively small spherical particles enclosed within a container. Kinetic energy is transmitted to the particles from the enclosure boundaries by collisional momentum exchange. As the energy flows to the particles, continuously changing particle–particle and particle-enclosure interactions result in energy being released from the system via inelastic impacts and interface friction.

Granular dampers are inexpensive and easy to retro-fit to a structure [1]. They are highly effective in reducing noise and vibration [2,3] and can maintain effectiveness under severe conditions, where most traditional damping techniques fail [4,5]. As a result, they are receiving increasing attention from researchers and have been successfully implemented in various engineering applications that include the automotive [3,5,6], electronic [7], aerospace [1,8,9], turbomachinery [4,10], and construction [11] sectors. However, the design of a granular damper is not an easy task [12] since they exhibit a high level of non-linearity that depends particularly on the vibration amplitude and is significantly affected by many parameters including cavity shape, fill ratio and particle properties [13–16]. Over the last two decades, there have been many studies that report the effects of these parameters on the damper performance, but because they focus on slightly different applications and configurations, findings appear inconsistent and sometimes contradictory. In

* Corresponding author.
E-mail addresses: fterzioglu1@sheffield.ac.uk (F. Terzioglu), j.a.rongong@sheffield.ac.uk (J.A. Rongong), c.lord@sheffield.ac.uk (C.E. Lord).

https://doi.org/10.1016/j.ymssp.2022.110038
Received 8 June 2022; Received in revised form 7 October 2022; Accepted 10 December 2022
Available online 17 December 2022

Table 1
Some principle motional phases identified in literature.

Phase name	Main characteristics	Vibration condition	Orientation relative to gravity		
			No gravity	90°	0°
solid-like	insignificant particle motion relative to the walls	very low amplitude	–	[21]	[26]
fluidised, activated	particles move relative to each other, but average relative positions are maintained	medium amplitude	–	[18,23]	[24,27]
Leidenfrost	a small number of highly energised particles support a dense particle cloud that appears to float without contacting the end-walls	high amplitude, high frequency	–	–	[20,26]
convection	particle mean positions move in patterns like those seen in fluid convection	high amplitude, high frequency	–	[18,28]	[19,29]
gas-like	particle positions and movements resemble random motion in a gas	very high amplitude and frequency	[22,30]	[18]	[20]
bouncing bed, collect-and-collide	all particles move together as a packed unit, alternately impacting the end-walls	high amplitude, low frequency	[22,30]	[23]	[24,25]

fact, the only rule that receives widespread acceptance is that the maximum achievable energy dissipation is directly related to the mass of particles present.

A number of studies have noted that the collective motional behaviour of the granular medium within the damper enclosure (usually referred to as the phase, state or mode) plays an important role in dissipating the vibrational energy of the system [17,18]. As summarised in Table 1, early work in this field identified different motional phases depending on the frequency and amplitude of excitation [18–21] and noted that the presence and direction of gravity plays an important role in the number and type of motional phases that occur [20,22,23]. Recognising that particle interactions (and therefore the resulting energy dissipation) are defined by the motional phase, more recent investigations have focused on identifying relationships between granular damping efficiency and motional behaviour to enable more efficient granular dampers to be designed [24,25].

Despite increasing interest, understanding relating to the damping effectiveness of different motional phases remains fragmented at present. The identification and naming of motional phases are inconsistent as are the measures used to quantify the effectiveness of the damping achieved. Additionally, findings often relate only to limited ranges of excitation as the focus of the research is guided by the need to address a particular application. However, from the literature, two motional phases are often identified as being interesting for granular damping. One of these is usually referred to as the “bouncing bed” and involves all the particles moving together as a packed unit, alternately impacting the end-walls of the cavity [22,30–32]. The other is loosely referred to as “fluidisation” and involves enough decompaction to allow sliding between particles without achieving fluid-like convectional motion [18,33,34]. Several other motional phases are consistently identified by different research teams and some of these are also thought to be effective zones for granular damper applications [19,24,25].

The aim of this work is to show how the phase map of a granular damper is directly related to its effectiveness in dissipating vibrational energy. This understanding is of great value when designing a granular damper as it provides context for any results generated, indicates the potential for improvement and enables estimation of sensitivity to changes in excitation. A clear understanding of the phase map for a particular damper therefore allows the designer to select parameter combinations that yield optimum performance in the expected operating conditions. This paper identifies the fundamental features of phase maps, making them easier to construct and therefore significantly reduces the effort required to design a granular damper.

2. Methodology

2.1. Approach

Phase maps were generated using three-dimensional numerical damper models subjected to sinusoidal vibration over a broad range of frequencies and vibration amplitudes. Motional phases were identified visually, based on particle movement at each excitation condition. A normalised measure of the corresponding energy dissipation was used to allow consistent comparisons to be made for differencing excitation conditions. The sensitivity of the results to the particle size, volume fill ratio and orientation with respect to gravity were also considered. Sensitivity to particle material properties or contact friction was not examined as their effects have been explained elsewhere [16,35] and are easier to account for.

Maps of motional phase in the frequency-amplitude space were compared visually with contour plots of normalised energy dissipation to demonstrate the link between them. More detailed investigations were also carried out to find the parameters that control the location of different phases, to simplify phase map estimation.

The study was conducted using simulations involving the Discrete Element Method (DEM) rather than physical experiments as this allowed greater control of the excitation conditions and specimen parameters while providing full-field detailed measurements. Extensive comparisons with experimental results were conducted but are not shown here as the DEM approach has been shown to be appropriate for granular damper studies by several other authors [16,36–38]. However, a limited validation study is presented to demonstrate the reliability of the results for the parameter ranges that were considered.

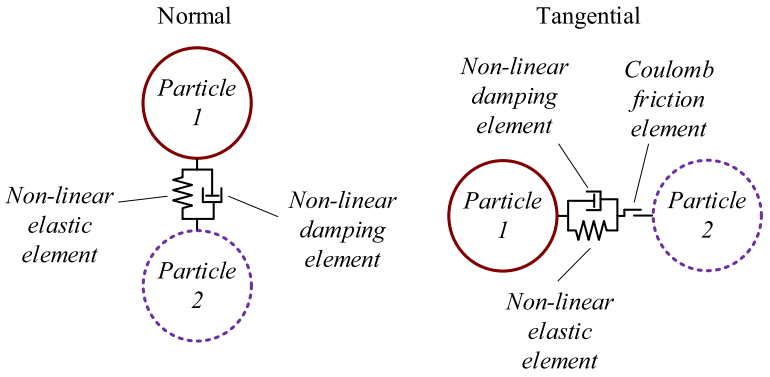

Fig. 1. Contact modelling of spherical particles.

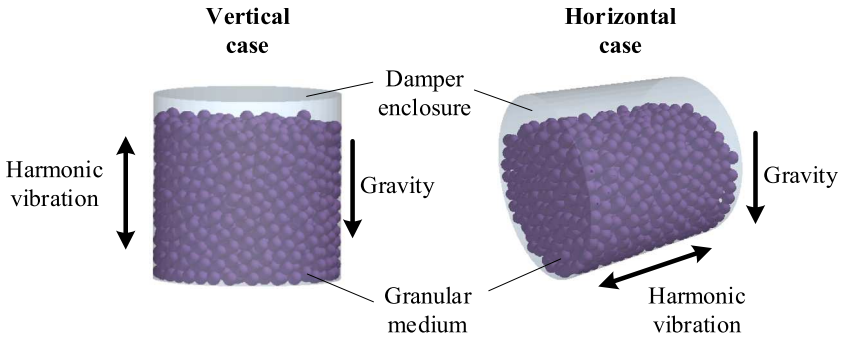

Fig. 2. DEM damper model for vertical and horizontal gravity-to-vibration orientations.

Table 2
The DEM simulation properties.

Cylindrical enclosure		Spherical particles	
Young's modulus	3.3 GPa	Young's modulus	3.3 GPa
Poisson's ratio	0.37	Poisson's ratio	0.37
Diameter	0.040 m	Density	1190 kg/m^3
Heights	0.040, 0.045, 0.050, 0.055 m	Nominal total mass	0.0279 kg
Volume fill ratios	0.466, 0.415, 0.373, 0.339	Diameters	3, 4, 5, 6 mm
		Number of particles	1659, 700, 358, 207
Contact and loading parameters			
Particle-enclosure friction coefficient	0.52		
Particle-particle friction coefficient	0.52		
Particle-enclosure restitution coefficient	0.86		
Particle-particle restitution coefficient	0.86		
Dimensionless accelerations investigated	1, 1.5, 2, 3, 4, 5, 6, 7, 8, 10, 12, 15, 20, 30, 40, 50, 60, 80, 100		
Frequencies investigated in Hz	20, 40, 80, 125, 160, 200, 320, 625, 1024		
Displacement amplitude range investigated	0.02 mm–62.12 mm		

2.2. Numerical modelling method

DEM is a numerical approach that enables modelling of the motion and interaction of large collections of discrete bodies (particles) and boundaries (enclosure walls). It explicitly calculates the displacements and rotations of every particle at discrete time points using a step size that is sufficiently small to maintain accuracy. All computed time steps constitute the full-time simulation history.

The principles of DEM were introduced by Cundall and Strack [39] and it has been successfully used in a number of research fields such as granular flow analysis, powder and rock mechanics, and crowd dynamics [40–42]. DEM has been found useful in granular damping investigations as it allows the user to control and observe both the contact conditions at particle level and the effects of these contacts on the overall energy dissipation [23,36–38]. Since the use of DEM is now mature, the authors limit their discussion on the theory of DEM. The detailed theoretical understanding of DEM can be found elsewhere [43,44].

In the DEM simulations carried out in this study, the deformation of each spherical particle was assumed small with respect to its

diameter. This means that particles are considered perfectly spherical when defining particle properties used in the equations of motion and identifying contact with other particles or the walls. At each contact point, the local elastic force–deformation behaviour was modelled employing the non-linear Hertz contact theory along the normal direction of contact whilst it was represented by the non-linear Mindlin-Deresiewicz approach in the tangential direction including Coulomb friction limitation force [41,42,45–48]. In a granular medium, contacts occur inelastically resulting in energy dissipation from collisions apart from inter-particle sliding friction. The level of inelasticity in a collision is most commonly expressed using the coefficient of restitution which can vary according to the material and the collision velocity [49–51]. In order to represent this dissipation Tsuji et al. proposed a non-linear approach [52] and found it to be consistent with experimental results [53–55]. A simple demonstration of the contact modelling approach between two particles is shown in Fig. 1.

2.3. Numerical granular damper model

The simulations carried out for this study used the commercial software, Altair EDEM [56], which is based on a three-dimensional DEM algorithm. Spherical particles were generated within a closed cylindrical enclosure as depicted in Fig. 2. Note that the results of this study are specific to enclosures whose side walls are perpendicular to the end walls.

The material properties of the particles and the enclosure used in this study are shown in Table 2 and were based on a typical acrylic polymer. Although many granular dampers use much harder particles (for example, steel or glass) the choice of a hard polymer was considered appropriate because the aim of this study was to compare the damping effectiveness of different motional phases rather than match a particular set of results or evaluate the material. Also, it has been shown extensively in literature that while material properties may affect the precise damping levels achieved, they do not change the overall trends in behaviour [35]. A practical advantage of using the properties of a polymer was that it increased the critical time step for the calculation (affected by the ratio of particle density to particle modulus) thereby significantly reducing the computational cost [57].

To assess the effect of particle size, four different spherical particle diameters were used in the simulations. To provide consistent analyses, the total mass of particles was kept constant for each damper configuration and so the number of particles reduced as their diameter increased. The enclosure dimensions were selected to display the main motional phases reported in literature. However, it should be noted that the findings of this study are valid regardless of enclosure dimensions as the motional phases are affected by the volume fill ratio of particles within the enclosure. Four different enclosure heights were used to investigate the effect of the volume fill ratio, which was specified as:

$$\upsilon = N_{\text{particle}} V_{\text{particle}} / V_{\text{enclosure}} \tag{1}$$

where N_{particle} is the total number of particles, V_{particle} is the volume of a particle and $V_{\text{enclosure}}$ is the enclosure volume. The full set of parameters used in this study is presented in Table 2.

Once the particles were initialised within the enclosure cavity in a random manner, a pre-simulation step was run for each condition considered. This lasted for 0.2 s and allowed particles to settle under the influence of gravitational acceleration. The simulation then involved prescribing the motion of the enclosure according to the function:

$$x = X\sin(\omega t) \tag{2}$$

Where X, t, and ω are the displacement amplitude, time and the vibration frequency (in rad/s), respectively. The vibration amplitude was specified in the form on the non-dimensional acceleration amplitude, described as:

$$\Gamma = X\omega^2/g \tag{3}$$

where g is the gravitational acceleration. For every condition considered, simulations were run at each frequency and each amplitude, as defined in Table 2. Note that the excitation ranges were consistent with literature [58,59]. Since the gravity-to-vibration directional orientation affects the occurrence of particular granular motional phases, the axial vibration was applied to the enclosure with the enclosure having two different orientation cases as illustrated in Fig. 2. It should be noted that only translational motion of damper enclosure is considered for both cases and, therefore, the findings of this paper are specific to the translational vibrations of granular dampers.

2.4. Granular energy dissipation calculation

Since DEM is time discretised, the total energy dissipated over a period of time can be obtained by summing the dissipation over every time increment considered. In this study, other sources of energy dissipation, such as viscous damping from the air, were assumed negligible. Thus, the dissipated energy over each time increment was computed using the dissipative contact forces.

$$\Delta E_{\text{dissipated}} = \sum_{i=1}^{N_{\text{particle}}} \sum_{j=1}^{N_{\text{contact},i}} \int_{T_{\text{contact},ij}} \left\{ \left| \boldsymbol{F}_{ij}^{nd} \cdot \boldsymbol{v}_{ij}^{n} \right| + \left| \boldsymbol{F}_{ij}^{td} \cdot \boldsymbol{v}_{ij}^{t} \right| \right\} dt \tag{4}$$

where $\mathbf{F}_{ij}^{nd}$ is the normal dissipative contact force and $\mathbf{F}_{ij}^{td}$ is the tangential dissipative contact force acting on particle i from its contacting body j; $\mathbf{v}_{ij}^{n}$ is the normal relative velocity and $\mathbf{v}_{ij}^{t}$ is the tangential relative velocity between the related contacting bodies. Here,

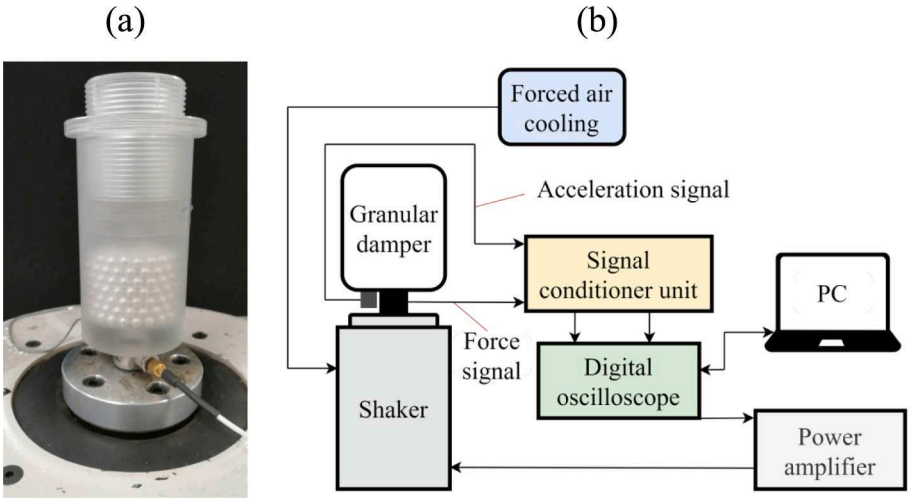

Fig. 3. The experimental testing setup: (a) damper model and (b) schematic representation of test rig and used equipments.

$N_{\text{contact},i}$ is the total number of contacts experienced by particle i; $T_{\text{contact},ij}$ is the contact duration of particle i with other contacting body j. It should be noted that the integration over the contact duration in Equation is performed as a sum-operation over small, discretised time steps.

Each simulation was run for 8 complete loading cycles and the last 5 periods were used to compute the dissipated energy so as to obtain steady-state dissipative behaviour. Checks showed that by ignoring the first 3 cycles, most transient effects could be eliminated.

Although energy is dissipated at every individual contact interaction, an average value was used to allow comparisons to be made more conveniently. One such measure that has been used elsewhere is the average dissipated power, which is calculated as:

$$\mathrm{P}_{\text{dissipated}} = \left\{E_{\text{dissipated}}(t + T_{\text{calculation}}) - E_{\text{dissipated}}(t)\right\}/T_{\text{calculation}} \tag{5}$$

where $T_{\text{calculation}}$ and $E_{\text{dissipated}}(t)$ are the dissipated energy calculation period and the total cumulative dissipated energy at the simulation time t, respectively.

Over the frequency and amplitude ranges considered, the power dissipation can vary by many orders of magnitude even for a linear damper, making comparisons difficult to visualise. Therefore, rather than using dissipated power itself, comparisons were made here using a granular damping efficiency parameter [22,30] defined as:

$$\epsilon_{\text{granular}} = 2\pi \mathrm{P}_{\text{dissipated}}/\omega \widetilde{\mathrm{E}}^{\max}_{\text{dissipated}} \tag{6}$$

where the maximum dissipated energy that can be achieved by a granular damper in a vibration cycle is defined with the equation given below:

$$\widetilde{E}^{\max}_{\text{dissipated}} = 4(\Gamma g/\omega)^2 \sum_{i=1}^{N_{\text{particle}}} m_i \tag{7}$$

where m_i is the mass of a particle. It should be noted that slightly different expressions for the maximum dissipated energy can be found elsewhere in literature [60,61]. However, as all the expressions only differ in terms of a constant scaling factor, the selected expression was considered sufficient for the comparative study.

3. Experimental validation of the DEM model

To demonstrate the appropriateness of the simulation, a set of equivalent physical experiments was carried out. A physical damper shown in Fig. 3a, with material properties and dimensions matching those used in the simulations, was filled with 358 particles, each with a diameter of 5 mm and a mean surface roughness of approximately 0.16 μm. Testing involved measuring the power dissipated by the damper as it was vibrated at a set of frequency and amplitude values [62]. The equipment and approach used here was the same as reported in previous work [16]. A simple schematic representation of the test rig can be found in Fig. 3b.

As shown in Fig. 3, the damper enclosure was mounted on an electrodynamic shaker. A force transducer was attached between the enclosure and the shaker to measure the force exerted on the damper as it underwent vibrational excitation. The resulting motion was measured using an accelerometer that was bonded to the bottom surface of the enclosure. Because tests were run at relatively high amplitudes for significant periods of time, a forced-air cooler was used to exhaust warm air from the shaker. While this prevented damage to the shaker, it is acknowledged that this was a potential source of high-frequency noise.

The excitation functions were generated via the personal computer (PC) and sent to the shaker via the digital-analogue converter in

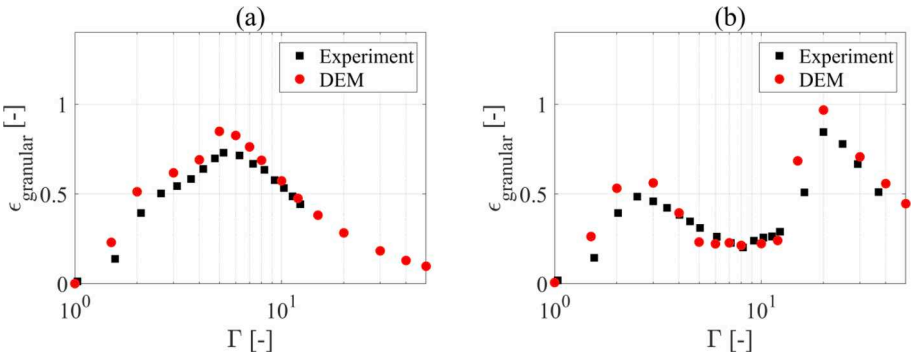

Fig. 4. Damping efficiency of experiment and DEM under vertical excitation where particle diameter is 5 mm and $\upsilon = 0.466$: at (a) 20 Hz and (b) 40 Hz.

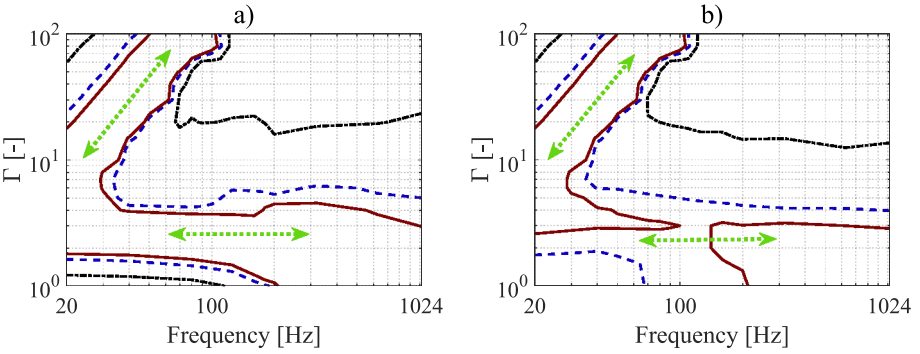

Fig. 5. Granular damping efficiency maps with particle diameter of 3 mm and $\upsilon = 0.466$ for (a) vertical and (b) horizontal cases: $\epsilon_{granular} = 0.1$ (), $\epsilon_{granular} = 0.3$ () and $\epsilon_{granular} = 0.4$ ().

the oscilloscope and the power amplifier. Analogue data from the accelerometer and the force transducer were conditioned and digitised (using a sampling frequency of 40 kHz) with the signal conditioner and the input channels of the oscilloscope, respectively. When the system was running and the damper had reached a steady-state condition, the captured electrical signals were converted to acceleration and force, using the associated transducer sensitivities, and stored on PC for further processing.

The experimental dissipated power in this testing setup is computed as [16,62]:

$$\left(P_{dissipated}\right)_{experimental} = \sum_{k=1}^{N-1} |\mathbf{F}_k||\mathbf{V}_k| \cos\left(\varphi_{\mathbf{F}_k} - \varphi_{\mathbf{V}_k}\right)/2 \tag{8}$$

where $\mathbf{F}_k$ and $\mathbf{V}_k$ are respectively the complex force and velocity at the frequency point k; $\varphi_{\mathbf{F}k}$ and $\varphi_{\mathbf{V}k}$ are the phase angles of complex force and velocity, respectively; and N is the total number of discrete frequency data points. Note that the frequency domain force and velocity can be obtained by applying the discrete Fourier transform for the measured force and acceleration signals. It should be also noted that the damping efficiency is obtained by writing the experimental dissipated power into Equation.

The resulting energy dissipation efficiencies are presented in Fig. 4. The two peaks in the 40 Hz data (Fig. 4b) represent the optimum conditions for two most important dynamic motional behaviours for energy dissipation, namely fluidisation and the bouncing bed. In the 20 Hz data shown in Fig. 4a, these two peaks coalesce somewhat. This result shows that the DEM simulations can accurately capture the most important granular dissipation behaviours. Experimental results were obtained for all the frequencies shown in Table 2 but are not presented here as they exhibited a similar level of correlation with the DEM results. However, for interested readers, experimental data relating to these tests can be obtained online [63].

4. Damping efficiency and observed motional phase maps

Results presented in the previous section show that the DEM simulations used in this work yield reliable results. This section presents results from simulations as they provide greater insight into particle motion and energy dissipation mechanisms than the associated experimental results would.

Fig. 5 shows the contour plots for granular damping efficiency as it varies with both frequency and amplitude. Only a few contour lines were used here to highlight the zones of low and high energy dissipation efficiency.

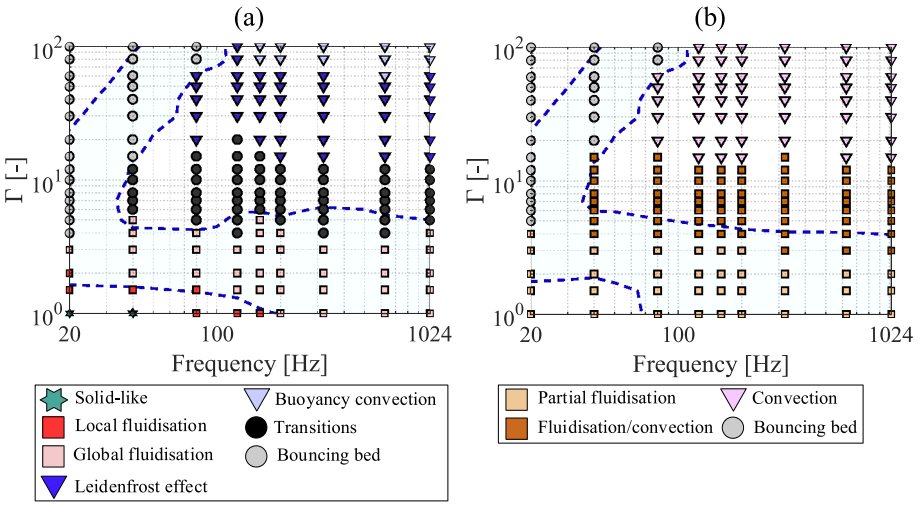

Fig. 6. Granular motional phase maps with particle diameter of 3 mm and $\upsilon = 0.466$ for (a) vertical and (b) horizontal cases – with lines of $\epsilon_{granular} = 0.3$ () showing high damping efficiency regions.

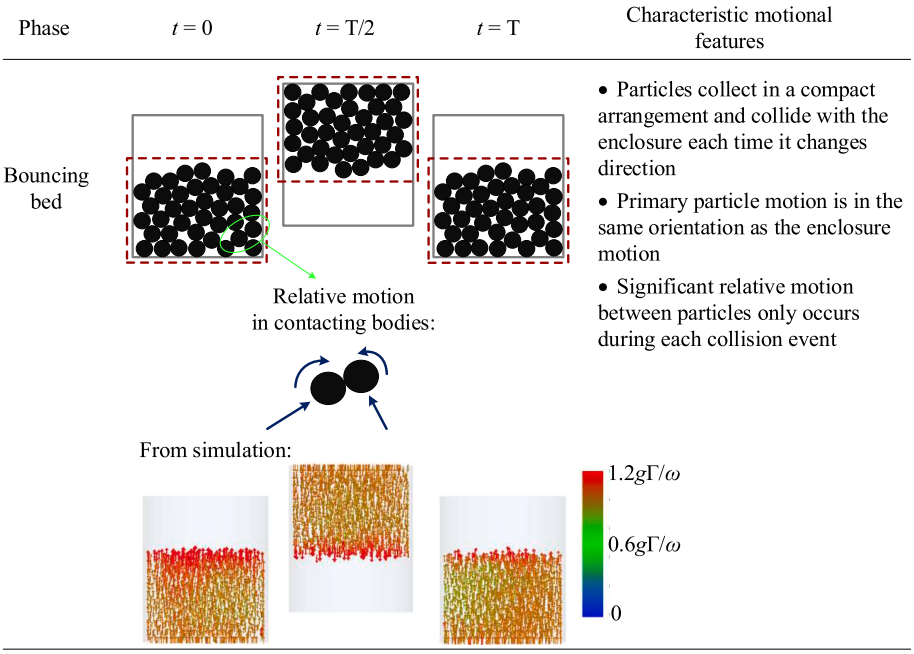

Fig. 7. Bouncing bed phase.

While there are minor differences between the damping efficiency maps for the two orientation cases, they have the same form. Both plots explicitly show two distinct areas of high energy dissipation effectiveness, noticeable as ridges (indicated by double-ended arrows) in the contour plots. One ridge runs diagonally from about $\Gamma = 6$ at 20 Hz to $\Gamma = 100$ at 90 Hz. The second ridge runs across the whole frequency range when the amplitude is around $\Gamma = 3$.

In this study, the granular motional phases were determined by visual observation of the particle movements from the recorded simulation animations and the individual particle velocity vectors from stored simulation histories for each excitation condition. The observed motional phase maps are presented in Fig. 6 using the same set of simulations as were used to create Fig. 5. Where possible, motional phase names and descriptions were kept consistent with those already used in literature. As transition between some phases was gradual rather than sudden, the phase name assigned for a particular excitation data point was selected from the type of dynamic motion that appeared to dominate. Note that some of the observed phases can be viewed as animations in Appendix A: Supplementary data.

Comparison of Figs. 5 and 6 shows immediately that the different damping efficiency zones relate directly to the different motional

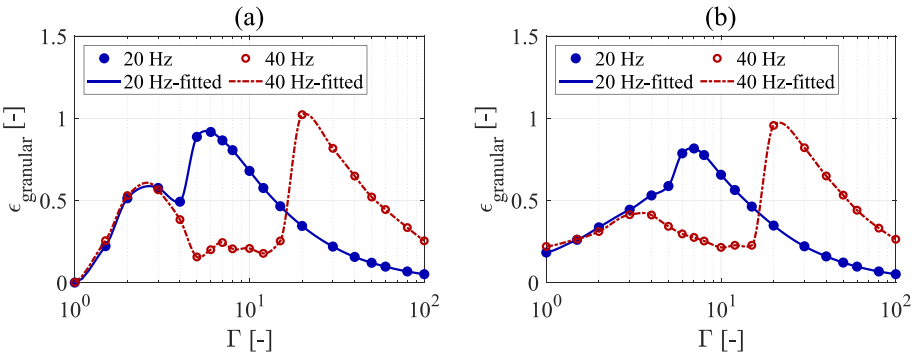

Fig. 8. Granular damping efficiency at 20 Hz and 40 Hz where particle diameter is 3 mm and $\upsilon = 0.466$: (a) vertical and (b) horizontal cases.

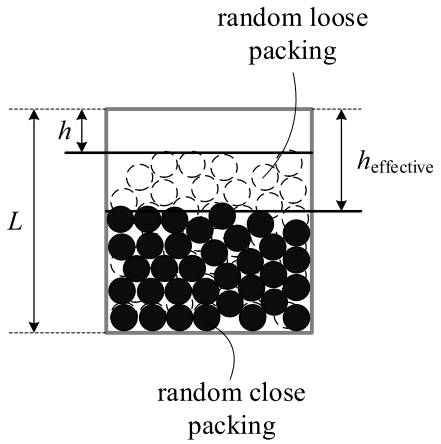

Fig. 9. Estimation of effective clearance.

phases. While the figures presented here are for one particular set of parameters, the results for all other volume fill ratios and particle sizes show similar damping efficiency and motional phase map relationships. Therefore, rather than present many similar-looking contour plots and phase maps, a discussion of the effects of these parameter changes for each particular motion type is presented.

As can be realised by comparing Figs. 5 and 6, the identified diagonal high energy dissipation effectiveness ridge is observed in the bouncing bed phase for both orientation cases. On the other hand, the frequency-independent high energy dissipation effectiveness ridge is seen in the global fluidisation for the vertical case and in the partial fluidisation for the horizontal case. The factors that affect the occurrences of these two ridges are different from each other.

4.1. Energy dissipation: the bouncing bed phase

The motional phase that has probably been the most extensively studied is the bouncing bed which is also sometimes referred to in literature as “two-sided bouncing bed” and “collect-and-collide” [22,23,30]. Fig. 6 shows that in the simulations carried out in this work, it is observed in regions of low frequency and high amplitude for both excitation orientation cases. Fig. 5 shows that this phase is the cause of the diagonal ridge defining a zone of high energy dissipation efficiency. In fact, this phase is often considered to be the optimal operating zone for granular dampers.

The bouncing bed phase involves the particles moving together in a closely packed arrangement and colliding alternately with each end of the enclosure. These collective collisions are synchronous: they occur twice per cycle at the time when the enclosure changes direction, as illustrated in Fig. 7 (see also Appendix A. Supplementary data).

Each collective collision has a relatively short duration, compared with the periodic motion of the enclosure, and involves a large transfer of momentum between the enclosure and the particles. These conditions instigate high contact forces and significant relative motion between the particles during the collective collision events resulting in high levels of energy dissipation. Between the collective collisions, the particles remain as a compact “bed” with negligible relative motion amongst the individual particles.

Previous studies into the energy dissipation effectiveness of the bouncing bed phase examined performance over a range of amplitudes [23,30,64]. They found that highest levels of effectiveness occurred at the onset of this phase: the lowest amplitudes that this phase exists for a particular frequency. It should be noted this is the optimum condition of collective collision for granular dampers. If the vibration amplitude is increased further, the resulting rise in dissipated power is less than the rise in input power which causes a

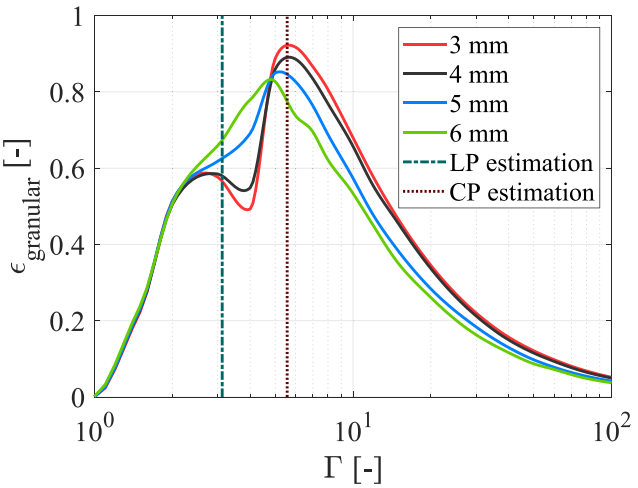

Fig. 10. Comparison of prediction approaches with varying particle size using the vertical 20 Hz simulation case presented in Fig. 8a.

Table 3
The optimum vibration amplitudes and estimations for diameter of 3 mm.

Volume filling ratio	Approach	20 Hz	40 Hz	80 Hz
0.466	DEM-vertical	5.7	20.8	83.8
	DEM-horizontal	6.8	21.5	83.4
	LP	3.1	12.5	49.9
	CP	5.6	22.3	89.0
0.415	DEM-vertical	8.4	30.6	>100
	DEM-horizontal	8.8	30.7	>100
	LP	5.7	22.7	90.9
	CP	8.1	32.5	130
0.373	DEM-vertical	10.9	50.1	>100
	DEM-horizontal	12.4	50.5	>100
	LP	8.2	33.0	132
	CP	10.7	42.8	171
0.339	DEM-vertical	13.8	52.2	>100
	DEM-horizontal	15.6	61.6	>100
	LP	10.8	43.2	173
	CP	13.3	53.0	212

decrease in the damper effectiveness.

The damping efficiency results from the simulation at 20 Hz and 40 Hz are shown in Fig. 8. As it can be seen comparing Figs. 6 and 8, the largest peaks occur around the bouncing bed onset amplitude and are independent from gravity-to-vibration orientation. Once the maximised efficiency is achieved, the damping efficiency decreases with increasing vibration amplitude. Nevertheless, the rate of this decrease is not as large as the increasing rate just before the peak as shown in Fig. 8 and demonstrated by others [30].

To predict the amplitude, at which the granular damper exhibits most efficient energy dissipation, Sack et al. estimated the collective collision time between the granular medium and the enclosure [22] and used it to develop the following relationship:

$$\Gamma_{optimum} = \omega^2 h / g\pi \tag{9}$$

Here, h is the clearance inside the damper as shown in Fig. 9 for the vertical case. They demonstrated the usefulness of this approach for a non-gravitational environment with frictionless particles and low frequencies up to 5 Hz. Meyer and Seifried considered this relationship for a wider range of frequency in a gravitational environment and also introduced the relative clearance definition to achieve a practical measure of the clearance [23]:

$$h/L = 1 - N_{particle} / \left(N_{particle}\right)_{max} \tag{10}$$

where L and $(N_{particle})_{max}$ represent the enclosure height and the maximum number of particles that can be fitted into the enclosure,

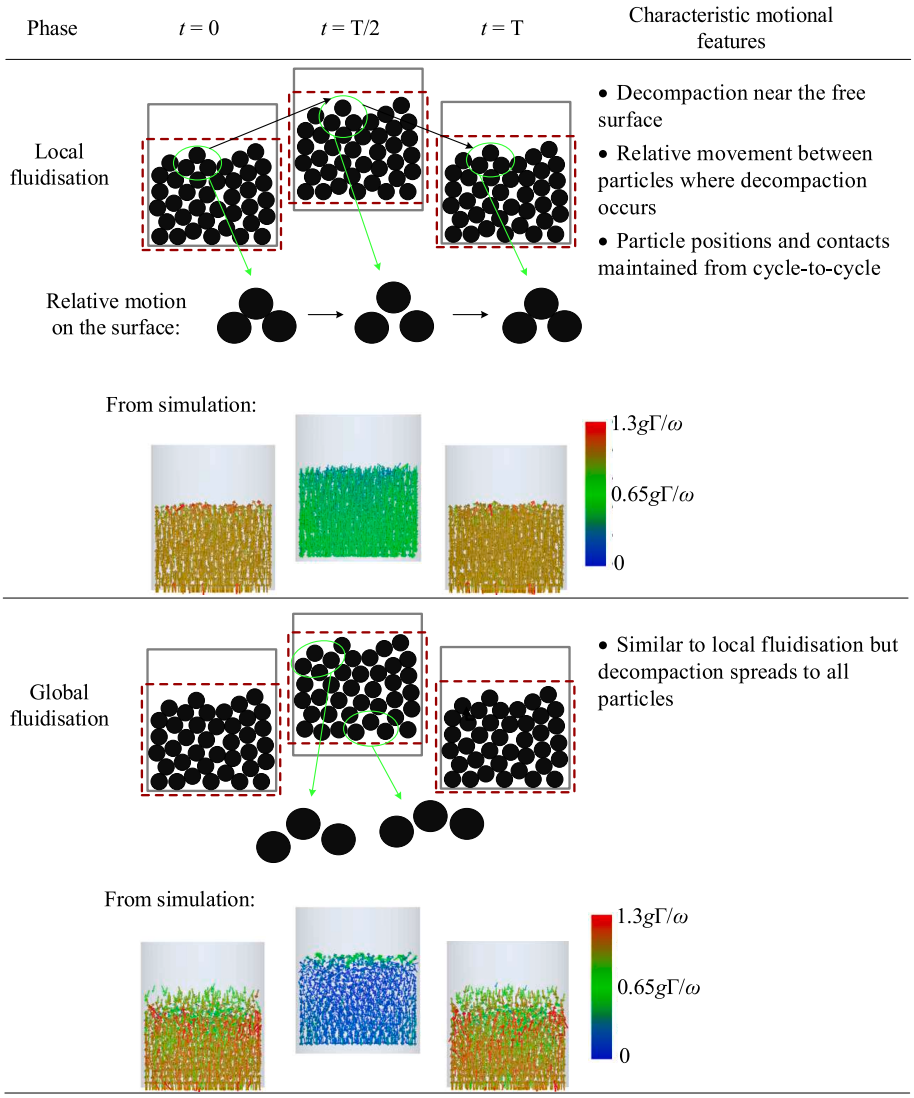

Fig. 11. Vertical fluidisation-based phases.

respectively. However, since the achievable maximum particle number can vary depending on particle packing arrangement and particle size, there were relatively large deviations between the measured and the estimated optimum amplitudes in their study.

When a cavity is filled under gravity but without any external vibration, the most probable arrangement is random loose packing, as illustrated in Fig. 9. However, during collective collisions in the bouncing bed phase, it was observed that the medium is compressed significantly, and particles move closer together, as indicated in Fig. 9. A more realistic estimation of the clearance requires this to be accounted for by replacing h with $h_{\text{effective}}$ in Eq. (9). The effective clearance is given by,

$$h_{effective}/L = 1 - \upsilon/\upsilon_{\max} \tag{11}$$

where $\upsilon_{\max}$ is the maximum achievable volume fill ratio in an enclosure which is nominally 0.64 for a random close packing of spherical particles, and can change depending on vibration amplitude and friction [65]. The maximum volume fill ratio has ranged between 0.53 and 0.58 (depending on particle size) in Meyer and Seifried's study [23]. This shows that their approximations were mostly based on random loose packing assumption in the enclosure, i.e., $\upsilon_{\max} \approx 0.55$ in Equation.

The close packing (CP) and loose packing (LP) estimations are illustrated for one typical case with the DEM simulation measurements with different particle sizes in Fig. 10. It shows that the CP estimation provides more accurate prediction for the peak in the bouncing bed phase. There is relatively little effect of particle size, the observed differences may relate to variability in packing particularly for the larger particles.

The estimation methods are compared with the DEM simulation measurements for all the volume fill ratios and three different frequencies in Table 3. Since the bouncing bed phase is observed at larger amplitudes for higher frequencies and the simulated

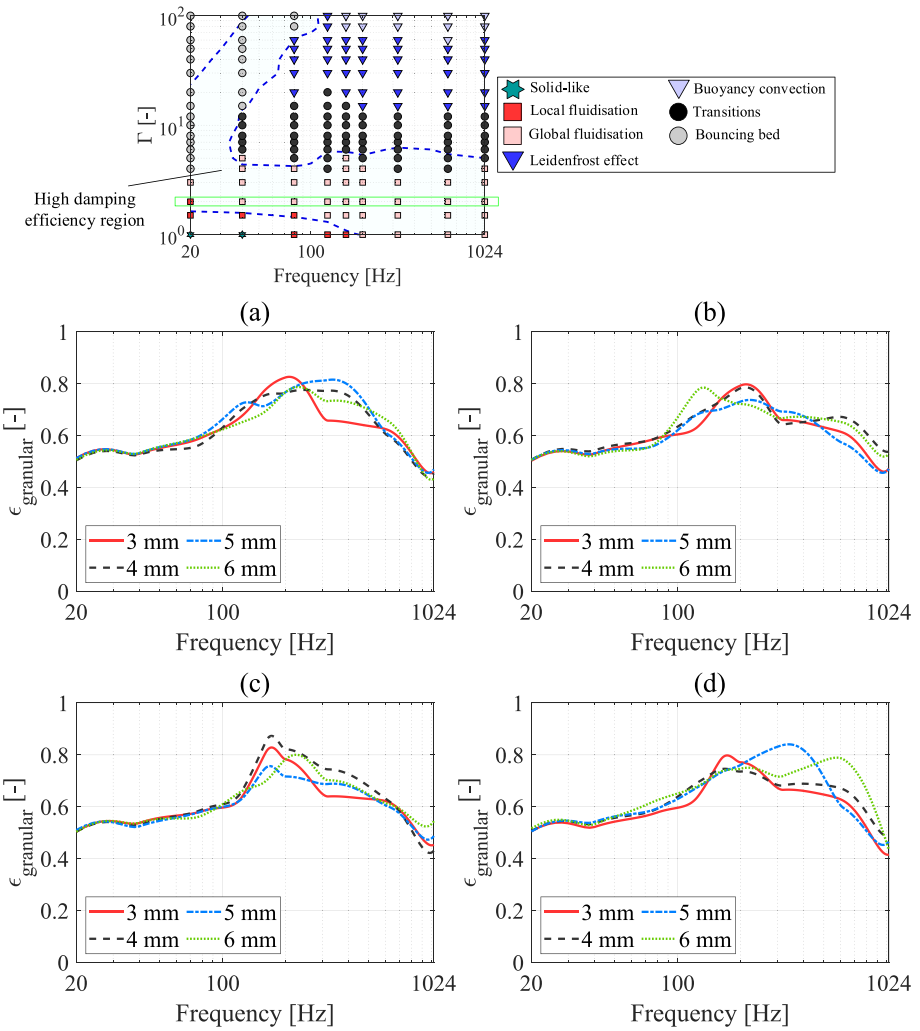

Fig. 12. Granular damping efficiency in vertical global fluidisation phase with varying particle size: (a) $\upsilon = 0.466$, (b) $\upsilon = 0.415$, (c) $\upsilon = 0.373$ and (d) $\upsilon = 0.339$.

amplitude resolution is lower at larger amplitudes, the uncertainty causes larger interpolation errors at higher frequencies in Table 3. It can be predicted from the Equation and seen in Table 3 that the optimum amplitude increases with frequency and clearance. It is apparent from Fig. 10 and Table 3 that the CP estimation provides more accurate estimations, while the LP significantly underestimates the optimum amplitude since it calculates the clearance lower than its actual value. Small differences between the CP estimate and the DEM results can be attributed to variations in the actual maximum packing fraction (assumed to be 0.64) and uncertainty in the peak values from the DEM results, which were obtained via logarithmic interpolation from the frequencies that simulations were run at.

4.2. Energy dissipation: fluidisation and convection based phases

The first motional behaviour seen in the vertical case is the solid-like phase – identified by green stars in Fig. 6a. This phase was observed when exciting the enclosure at $\Gamma = 1$ and the lowest frequencies (20 Hz and 40 Hz). Here, the particles behave like a solid mass fixed onto the enclosure base that moves with the same velocity as the enclosure. No noticeable relative motions exist amongst the particles or relative to the enclosure as the inertial forces generated from the excitation remain smaller than the restraining forces from gravity and friction. Energy dissipation from contact interactions is therefore negligible. This can be seen clearly in Fig. 5a. The solid-like motion does not occur in zero-gravity situations as there is no force to hold the particles together [64]. Although this behaviour has also been observed in horizontal excitations [21], it was not seen in this study, because simulations were not run at amplitudes below $\Gamma = 1$. Granular dampers are usually expected to operate beyond this phase (i.e., only once "activated") although it has been shown [66] that useful damping in this motional phase can be achieved using particular configurations of high-loss particles that maximise strain within the particles.

The term "fluidisation" is used in literature to refer to several different types of granular motion. In this study, the term is used to

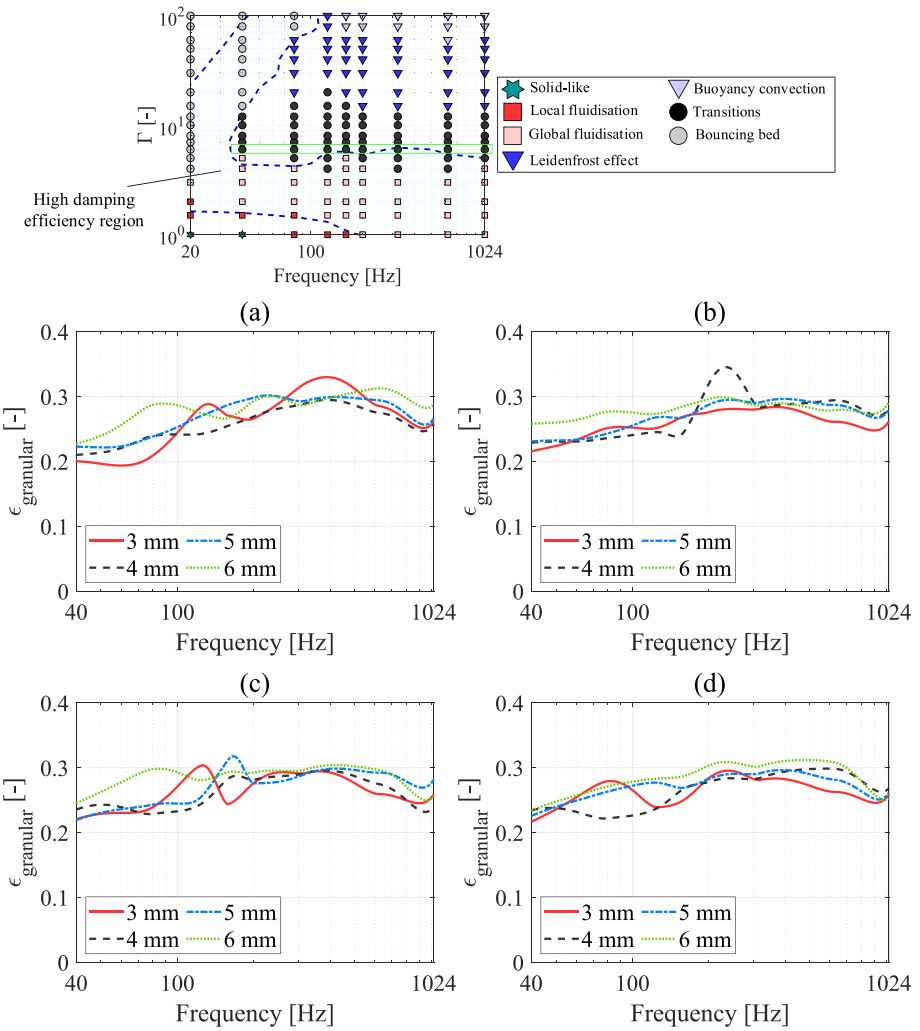

Fig. 13. Granular damping efficiency in vertical transition-1 with varying particle size: (a) $\upsilon = 0.466$, (b) $\upsilon = 0.415$, (c) $\upsilon = 0.373$ and (d) $\upsilon = 0.339$.

indicate the conditions where touching particles temporarily lose contact and move relative to each other but, over a full vibration period, approximately preserve their average positions and existing contacts. Four variations of fluidisation-based motional phase are identified in Fig. 6 and (by comparison with Fig. 5) can be seen to relate to the zone of high dissipation that occurs at amplitudes below $\Gamma = 5$ over the full range of frequencies.

At mid and high frequencies when the acceleration amplitude is also high, the particles become highly energised and exhibit significant convective motion. In granular systems, "convection" is associated with significant decompaction that allows the particles to move relative to one another. Additionally, when convection occurs, particles are transported to different locations of the enclosure and this motion often involves a significant component perpendicular to the excitation direction. Normally, the velocity magnitudes within the convection zone are small in comparison with those of the enclosure. Under these conditions, contact events are less severe and as a result, dissipated energy effectiveness is relatively low. In the simulations run in this study, significant convection is noticeable in three distinct phases: convection in the horizontal case and the Leidenfrost effect and buoyancy convection phases in the vertical case.

It should be noted that the three mentioned granular motion types (i.e., solid-like, fluidisation and convection) are in an inter-related gradual transition process depending on vibration amplitude. Therefore, it can be simply said that the granular motional phases change depending on the developing and disappearing of fluidisation behaviour within the granular medium excluding the bouncing bed phase. Here, this gradual transition is related with the observed energy dissipation effectiveness of granular dampers.

4.2.1. Vertical motion

In vertical motion, as the vibration intensity is increased, the solid-like phase gives way to the local fluidisation phase introducing fluidisation behaviour in the granular medium as can be seen in Fig. 6a. In this phase, the block of particles is first accelerated upwards by the enclosure base due to collective collision. During the vibration cycle, as the deceleration of the enclosure is greater than that of

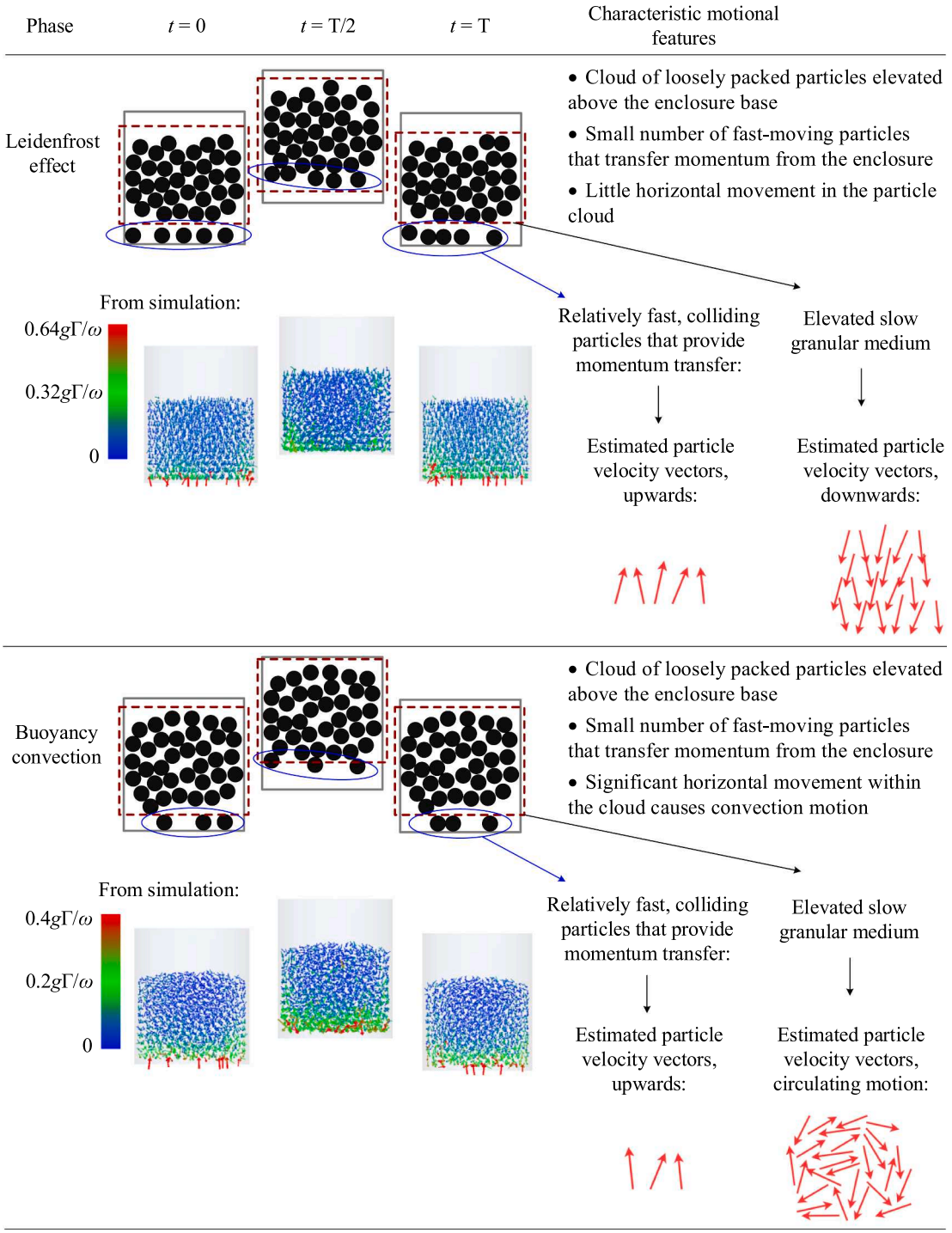

Fig. 14. Vertical convection-based phases.

gravity, the particles tend to lift relative to it resulting in decompaction and relative motion, particularly near the free surface at the top where the particles are least restrained. At the end of the cycle, the particles again collide with the enclosure base and the process repeats. This local fluidisation behaviour in the uppermost particle layers is illustrated in Fig. 11. Since the momentum exchange is essential for a granular damper to dissipate vibrational energy, the local fluidisation can be regarded as the first phase in which energy dissipation occurs in the vertical case.

As the vibration intensity increases further, fluidisation behaviour spreads from the uppermost particle layers downwards through

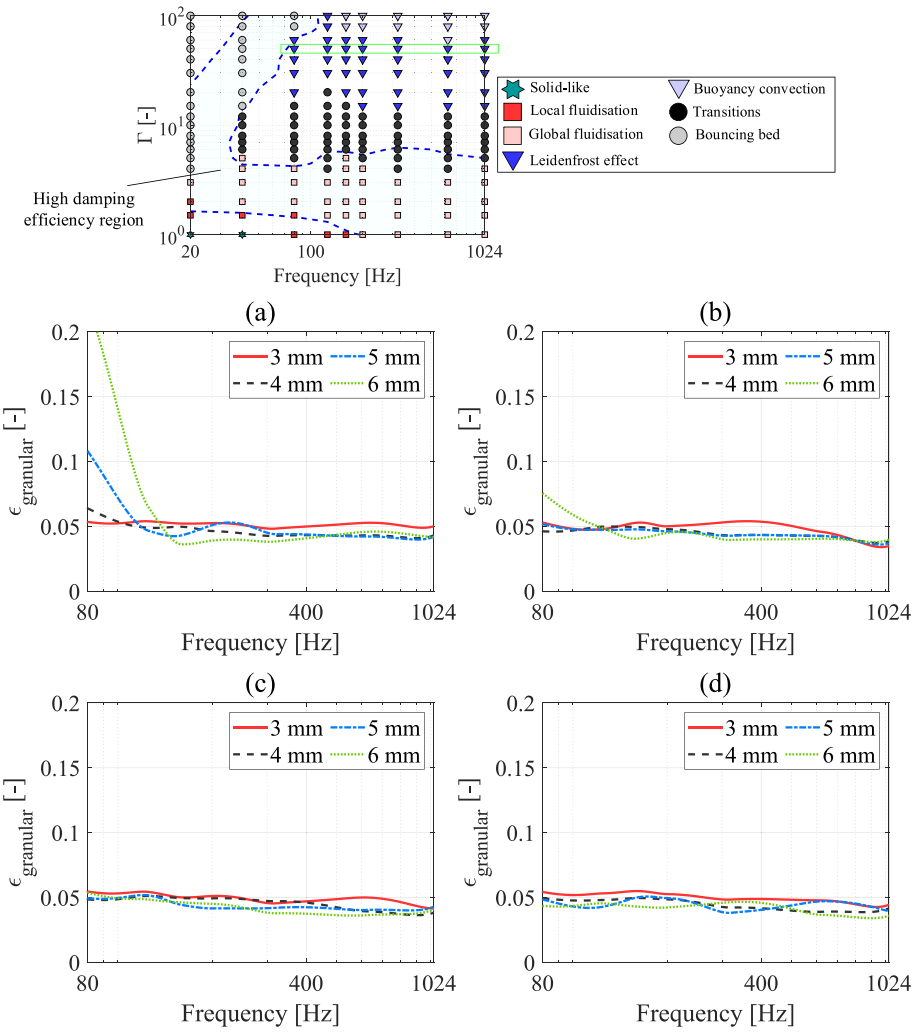

Fig. 15. Granular damping efficiency in vertical Leidenfrost effect with varying particle size: (a) $\upsilon = 0.466$, (b) $\upsilon = 0.415$, (c) $\upsilon = 0.373$ and (d) $\upsilon = 0.339$.

the whole body of particles, leading to increased energy dissipation. This condition is referred to as the global fluidisation and is illustrated in Fig. 11 (see also Appendix A. Supplementary data). The global fluidisation provides effective granular damping over a wide frequency range for relatively small vibration amplitudes – see Fig. 12. Close inspection of Fig. 6a shows that the lower boundary for the global fluidisation drops somewhat as the frequency increases demonstrating that this effective damping can be achieved at lower acceleration amplitudes for high frequency vibrations. As the vibration amplitude increases while operating in the global fluidisation, convective motion starts gradually initiating within the granular medium which causes reductions in energy dissipation effectiveness.

The sensitivity of damping effectiveness in this phase to particle diameter and volume fill ratio is presented in Fig. 12. Here, the green box in the phase map shows the location of the datapoints used to generate the damping efficiency plots. These plots show that the effectiveness of this phase is not notably affected by particle size or volume fill ratio. The slight rise in the values for all curves around 200 Hz is due to the proximity of the selected datapoints to the nominal optimum condition where the whole granular medium is fluidised.

When the vibration amplitude is further increased after the optimum condition in vertical excitation, the occurrence of fluidisation behaviour reduces, and they are replaced by some convection motions. First, a transitional phase, where particle motion does not repeat with each oscillation of the enclosure, is observed (see Appendix A. Supplementary data). This transitional phase is identified as being between the global fluidisation and the Leidenfrost effect as can be seen in Fig. 6a, and it results in only one significant impact period every-two vibration cycles. There is a second transitional phase occurred just before the bouncing bed motion is appeared, and it involves a collective collision with the upper wall of the enclosure only once every-two vibration periods. However, as the latter transition phase only occurred at very few excitation points, it is not considered in this work and will be investigated in a future study.

In the first transition phase, a significant energy dissipation efficiency is evident as shown in Figs. 5a and 13. This may be because

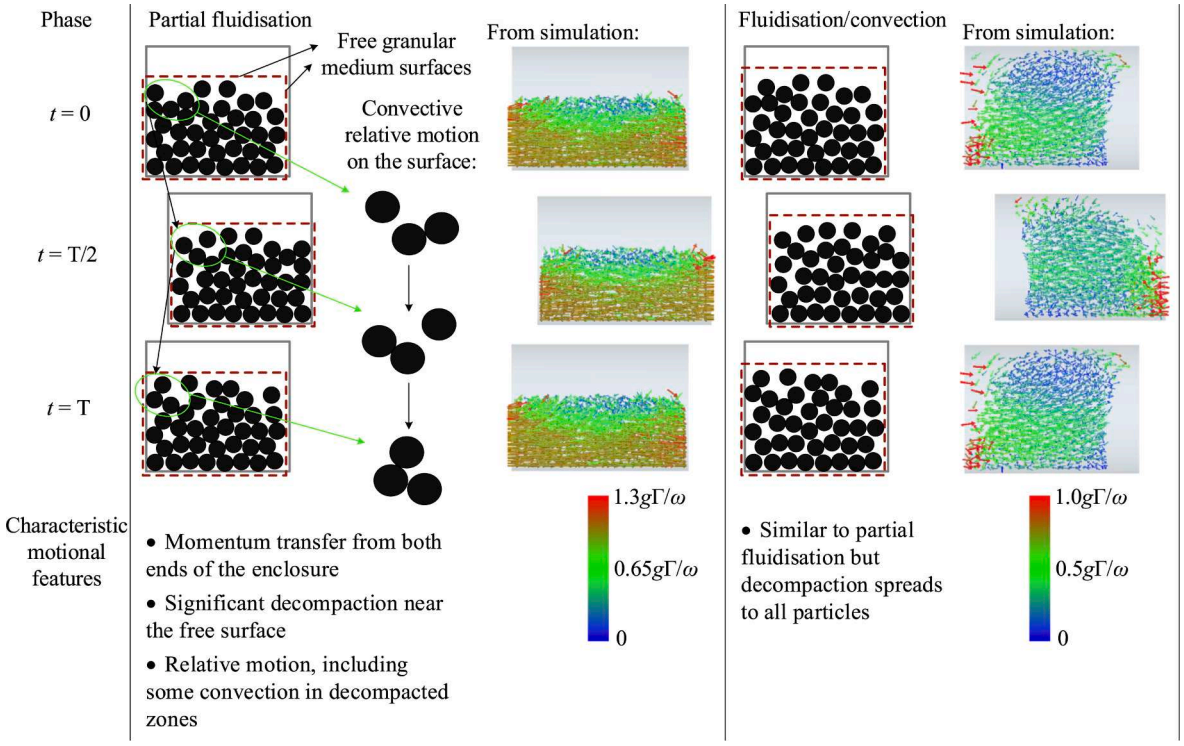

Fig. 16. Horizontal fluidisation-based phases.

the ratio of fluidised particle motion to convective motion remained relatively high. It can be said that the energy dissipation effectiveness in this phase is almost insensitive to frequency, particle size and volume fill ratio.

The energy dissipation efficiency in this phase appears to fluctuate more than in other phases as can be seen in Fig. 13. One explanation is that in this phase, the proportion of convection-based motion is much more sensitive to the excitation frequency. The other is that in the transition phases, collective collisions (between the body of particles and the enclosure) differ in number and intensity from one cycle to the next and therefore, the number of cycles used to evaluate the average energy dissipation in this study was inadequate at some excitation cases for this phase.

In vertical motion, under high frequency and amplitude excitations, convection motion obtains the dominancy in the granular medium, and as a result, convection-based motional phases occur, and they are referred to as the Leidenfrost effect and the buoyancy convection. The Leidenfrost phase is the dominant motion type in Fig. 6a over the amplitude range $15 < \Gamma < 80$ and the frequencies above 80 Hz. In this phase, the particles form a loosely packed cloud that is lifted above the enclosure base throughout a vibration cycle, as shown in Fig. 14 (see also Appendix A. Supplementary data). This cloud, made up of slow-moving particles, remains at a steady height relative to the enclosure base. Its position is maintained by a relatively small number of fast-moving particles that are located at its lower surface and have collisions with the enclosure base when it is close to the lowest position. Fig. 14 also shows vertically oriented motion for the fast-moving particles and those in the cloud around the time that they collide ($t = 0$ and $t = T$ in Fig. 14). This generates horizontal homogeneity in the granular medium [19].

At higher vibration accelerations, the Leidenfrost phase gives way to the buoyancy convection as seen in Fig. 6a. In this phase, as shown in Fig. 14, the volume of particle cloud expands, and the top particle layers form a curved shape rather than an approximate flat surface. The velocity vector directions within the particle cloud are no longer just oriented vertically at the collision times but show that significant rolling convective motions take place. The cause for this breakdown of horizontal homogeneity in the particle cloud may be due to the increased velocity of the high-speed particles. As they transfer momentum to the particle cloud, it expands creating more gaps which increases the likelihood of more oblique impacts, which in turn cause more transverse motion and rolling.

The energy dissipation effectiveness in the Leidenfrost phase (see Fig. 15) is relatively low compared to the fluidisation-based phases and the mentioned transition phases. Granular damping efficiency also remains low in the buoyancy convection phase. The likely reason for low dissipation effectiveness is a lack of efficient momentum transfer to the particle cloud, as this only occurs via the small number of high-speed particles. Although some papers have identified the Leidenfrost effect [19] and the buoyancy convection [25] as the optimal motional phase in vertical excitation, this current study does not appear to support their conclusions. However, it is interesting to note that the energy dissipation performance is insensitive to frequency, particle size and volume fill ratio and may therefore be useful in some design scenarios. Note that the increased dissipation effects near 80 Hz in Fig. 15 are caused by closeness to the bouncing bed phase, which has high energy dissipation efficiency as mentioned before.

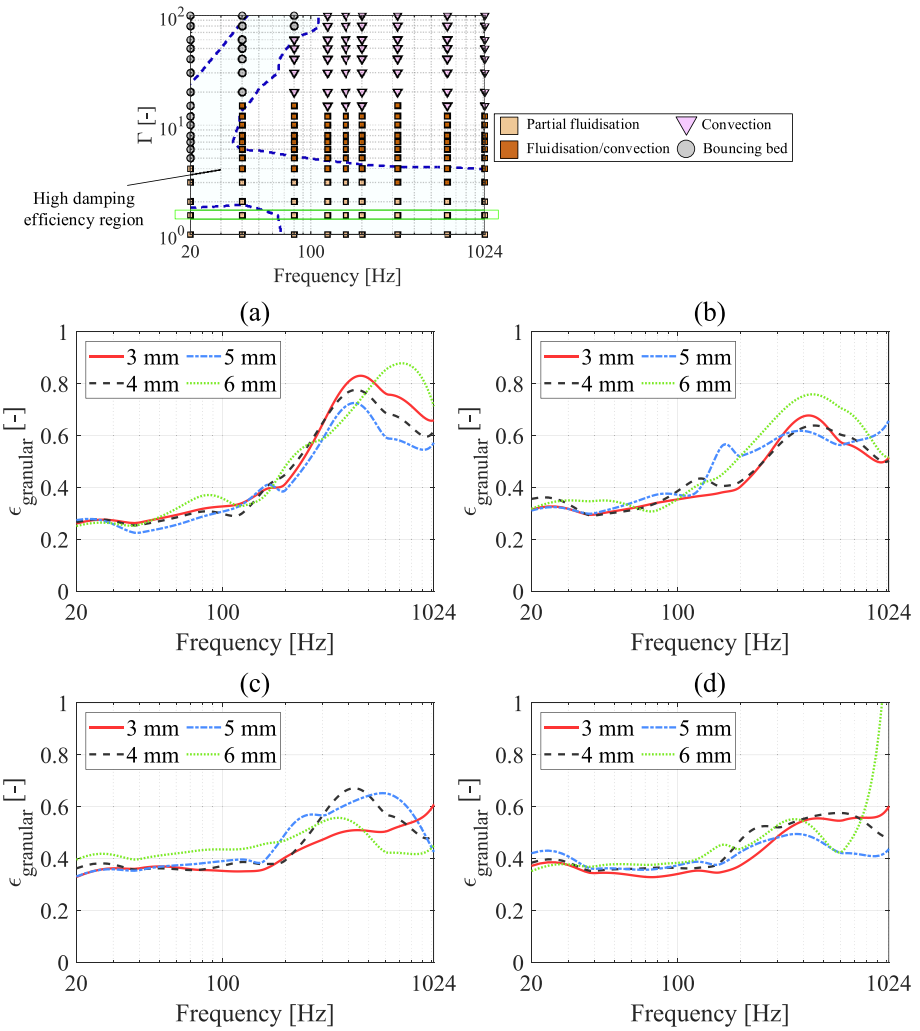

Fig. 17. Granular damping efficiency in horizontal partial fluidisation phase with varying particle size: (a) $\upsilon = 0.466$, (b) $\upsilon = 0.415$, (c) $\upsilon = 0.373$ and (d) $\upsilon = 0.339$.

4.2.2. Horizontal motion

Fluidisation behaviour is also observed in horizontal excitations but because the gravity and the enclosure motion are perpendicular to each other, there are a few differences in the ways that the particles move. Horizontal fluidised motion can also be separated into two phases as illustrated in Fig. 16. Although these phases are sometimes also called "local fluidisation" and "global fluidisation" in literature, they are referred to here as "partial fluidisation" and "fluidisation/convection" to avoid confusion with the vertical case which have the same names but different motional behaviours. In the horizontal fluidisation-based phases, momentum transmission occurs at both ends of the enclosure. Gravity causes the collection of particles to rest on the lower wall of the enclosure and creates a free surface parallel to the principal motion direction. This difference generates some convectional behaviours where the particles permanently lose their existing contacts by changing their overall positions during a vibration period. Therefore, it can result a lower energy dissipation effectiveness in the horizontal case than the vertical case at the optimum fluidisation condition – it can be seen in the small peaks shown in Fig. 8.

In the partial fluidisation phase, convective behaviours occur near the upper free surface while on the lower surface (in contact with the enclosure) motion is similar to that seen in the solid-like phase. Energy dissipation efficiency is moderately high, as can be realised from Fig. 5b and Fig. 6b. Sensitivity to the particle size and volume fill ratio is presented in Fig. 17. It can be seen that the granular damping efficiency generally remains independent of the particle size but increases somewhat towards higher frequencies if the volume fill ratio is high. This could be related to the higher proportion of fluidisation behaviour at higher frequency excitations in this phase. As the volume fill ratio grows, the damping efficiency level at lower frequencies decreases and the mentioned difference between lower and higher frequencies increases.

As the vibration intensity is increased, fluidisation behaviour increases. However, zones of convective behaviour also extend deeper into the particle collection, hence the use of the term fluidisation/convection to describe this motion. The energy dissipation

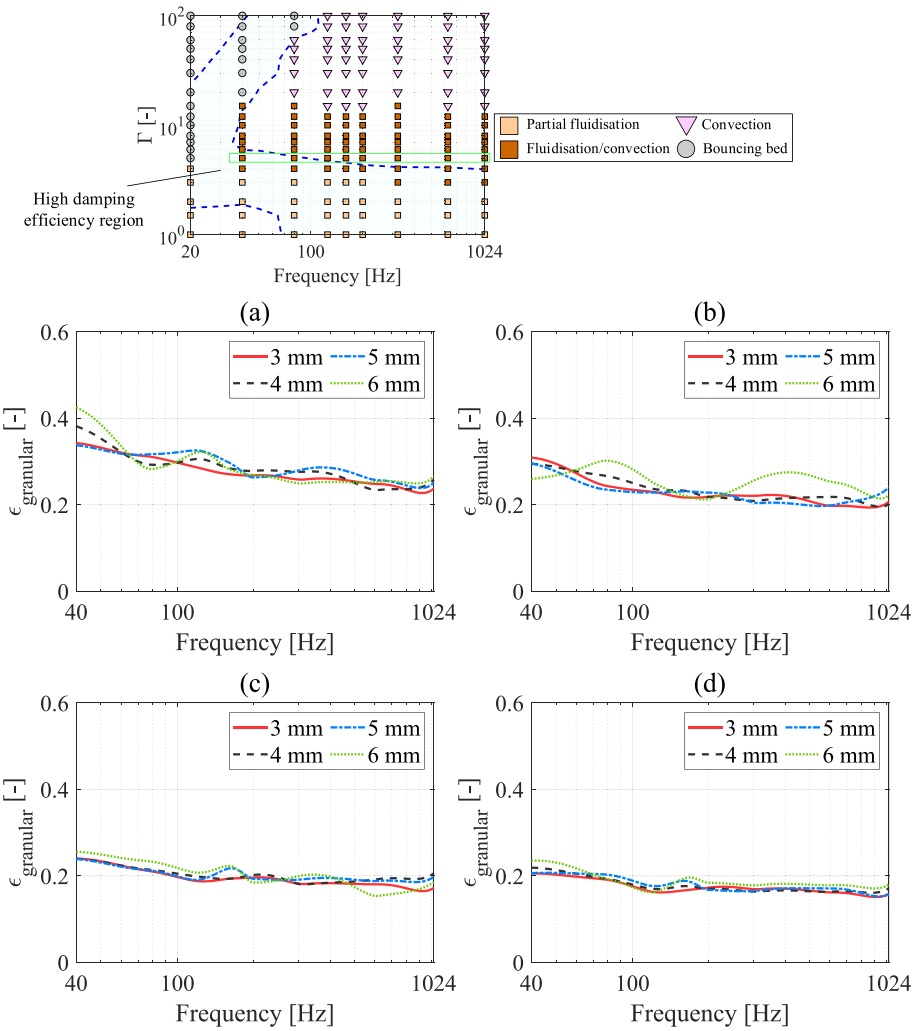

Fig. 18. Granular damping efficiency in horizontal fluidisation/convection phase with varying particle size: (a) $\upsilon = 0.466$, (b) $\upsilon = 0.415$, (c) $\upsilon = 0.373$ and (d) $\upsilon = 0.339$.

effectiveness is shown in Fig. 18 for varying parameters. As seen with the partial fluidisation, particle size does not affect the energy dissipation performance in this phase. However, increased clearance reduces the effectiveness. The most likely reason for this is that greater clearance allows the particles to spread further in a horizontal direction, reducing the depth and therefore making convection motion more likely in the granular medium. As convective motion is associated with low energy dissipation efficiency, the overall energy dissipation effectiveness level decreases. As contrary to the investigated partial fluidisation case, slight decreasing in the effectiveness with increasing frequency was observed in this phase.

Under horizontal motion, some convection occurs in the fluidisation-based phases and the more convection there is, the lower the damping efficiency. With increased vibration intensity, the convection phase is reached (identifiable in Figs. 5b and 6b for higher frequencies when $\Gamma > 15$) where most of the particles undergo convection motion. In this phase, there is significant decompaction, and fast-moving particles occur at both boundaries of particle cloud as shown in Fig. 19.

Levels of granular damping efficiency were found to be very low – as illustrated in Fig. 20 and slightly decreases along the frequency axis. Increased clearance slightly reduces the effectiveness, but the particle size does not affect the energy dissipation performance. Note that the high levels seen at the lowest frequencies are due to being close to a different motional phase.

4.3. General discussion on effectiveness of motional phases

Effective damper design depends on the application, the host structure and external loading conditions. A damper that is highly effective in reducing the vibrations of one structure will not necessarily be effective when applied to a different structure as success depends not only on having an adequate mass of particles but on ensuring that they function effectively. Effective functioning of a damper is defined by the motional phase of the particles when subjected to the operational vibrations. Thus, achieving a suitable

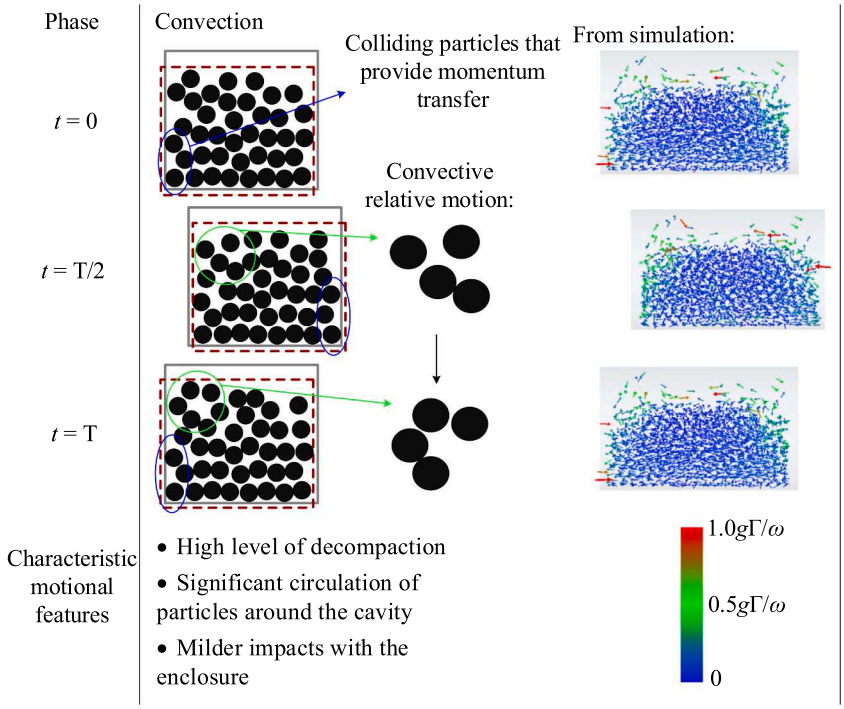

Fig. 19. Horizontal convection phase.

motional phase is critically important in damper design.

From the findings discussed in this section, the following general design rules can be defined:

I. If the operating frequency range is relatively narrow, the bouncing bed phase will offer the highest damping level over a relatively large amplitude range. The key design parameter is the effective clearance which can be calculated from Equation. This is also the only effective phase for zero gravity conditions [22,30].
II. For a wide frequency range at relatively low amplitude, the fluidisation phases (global fluidisation for the vertical case and partial fluidisation in the horizontal case) will give best performance. The amplitude for optimum performance can be adjusted by altering the static pressure field for example, by making the particle bed deeper and narrower [15,18,23].
III. If excitation amplitudes are beyond highest-amplitude optimum zone that can be achieved for fluidisation phases, the transition phase (in the vertical case) and fluidisation/convection (in the horizontal case) can also be employed, although the damping achieved will be somewhat lower.

5. Conclusions

The aim of this study was to relate the granular motional phase map to energy dissipation effectiveness for a broad range of conditions. This was achieved using a DEM model validated by experimental work. A clear link between the phase map and energy dissipation has been shown and explanations provided of how the different motional phases cause energy dissipation.

The work has shown that there are two distinct mechanisms that control the performance of granular dampers: collective collision and fluidisation. Optimal performance can be achieved for each mechanism, but they are affected by different factors. Some of the apparent contradictions in the literature can be explained by referring to the dominant mechanism involved in that particular piece of work.

The most effective collective collision regime involves two collisions per cycle that occur at alternate ends of the enclosure (the “bouncing bed” phase). This phase provides the highest energy dissipation efficiency, but the optimum conditions occur over a narrow range, which appears as a diagonal ridge on a frequency-amplitude map. This work has shown that the location of this optimum condition can be accurately estimated by determining the effective clearance in the damper and relating this to the operating amplitude and frequency because of the link between flight time of the particle group and the motion of the casing. It was shown that random close packing within the particle group gave the best estimate of effective clearance – an important finding because the optimum zone in this phase is relatively narrow.

While the existence of the solid–fluid-convection process exhibited by a granular medium is well known, this paper has shown that it is independent of collective collision regime, so that it can be optimised separately. Behaviour is affected primarily by the level of activation (relative level of dynamic and static forces) and the optimum dissipation effectiveness occurs when the majority of particles

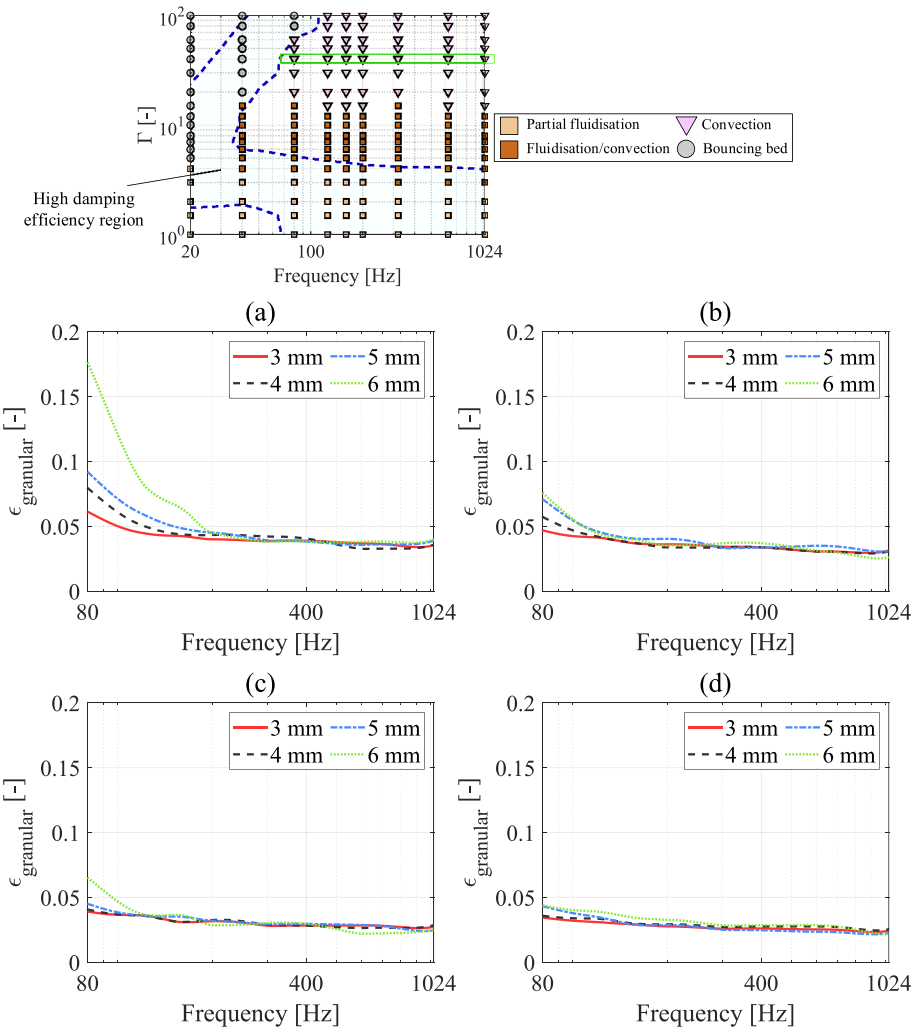

Fig. 20. Granular damping efficiency in horizontal convection phase with varying particle size: (a) $\upsilon = 0.466$, (b) $\upsilon = 0.415$, (c) $\upsilon = 0.373$ and (d) $\upsilon = 0.339$.

are fluidised but have not yet started to convect. Optimum conditions were found to be relatively insensitive to frequency, they are identifiable as a broad ridge on the amplitude-frequency map at normalised acceleration of around $\Gamma = 3$. This work suggests that optimised fluidisation-based phases can be used for low-amplitude, frequency-independent granular damper designs.

Away from optimal collective collision or fluidisation, the granular energy dissipation effectiveness reduces. Particle size was not found to affect dissipation behaviour significantly. The enclosure length affects the collective collision mode only in terms of the clearance distance, and the fluidisation behaviour in terms of the particle bed depth and hence level of activation.

The significance of the work presented in this paper is that it simplifies the design process of granular dampers. The designer is presented with the choice either to optimise collective collision (if the expected amplitude and frequency are well-defined) or to optimise fluidisation (for performance over a broad frequency range). The phase map can then be used to assess the benefits of potential changes without the need for further numerical or experimental sensitivity studies, greatly reducing the effort expended.

Declaration of Competing Interest

The authors declare that they have no known competing financial interests or personal relationships that could have appeared to influence the work reported in this paper.

Appendix A. Supplementary data

Supplementary data to this article can be found online at https://doi.org/10.1016/j.ymssp.2022.110038.

References

[1] H.V. Panossian, Structural damping enhancement via non-obstructive particle damping technique, J. Vib. Acoust. 114 (1992) 101–105, https://doi.org/10.1115/1.2930221.
[2] Z. Xu, M. Yu Wang, T. Chen, A particle damper for vibration and noise reduction, J. Sound Vib. 270 (2004) 1033–1040, https://doi.org/10.1016/S0022-460X(03)00503-0.
[3] L. Hu, Y. Shi, Q. Yang, G. Song, Sound reduction at a target point inside an enclosed cavity using particle dampers, J. Sound Vib. 384 (2016) 45–55, https://doi.org/10.1016/j.jsv.2016.08.016.
[4] J.J. Moore, A.B. Palazzolo, R. Gadangi, T.A. Nale, S.A. Klusman, G.V. Brown, A.F. Kascak, A forced response analysis and applicationof impact dampers to rotordynamic vibration suppression in a cryogenic environment, J. Vib. Acoust. 117 (1995) 300–310, https://doi.org/10.1115/1.2874452.
[5] F. Duvigneau, S. Koch, E. Woschke, U. Gabbert, An effective vibration reduction concept for automotive applications based on granular-filled cavities, J. Vib. Control. 24 (2018) 73–82, https://doi.org/10.1177/1077546316632932.
[6] S. Koch, F. Duvigneau, R. Orszulik, U. Gabbert, E. Woschke, Partial filling of a honeycomb structure by granular materials for vibration and noise reduction, J. Sound Vib. 393 (2017) 30–40, https://doi.org/10.1016/j.jsv.2016.11.024.
[7] P. Veeramuthuvel, K.K. Sairajan, K. Shankar, Vibration suppression of printed circuit boards using an external particle damper, J. Sound Vib. 366 (2016) 98–116, https://doi.org/10.1016/j.jsv.2015.12.034.
[8] B. Knight, D. Parsons, A. Smith, Evaluating attenuation of vibration response using particle impact damping for a range of equipment assemblies, in: AIAA Aerosp. Des. Struct. Event, Boston, Massachusetts, 2013: pp. 1–9.
[9] S.S. Simonian, Particle damping applications, in: 45th AIAA/ASME/ASCE/AHS/ASC Struct. Struct. Dyn. Mater. Conf., Palm springs, California, 2004: pp. 4145–4161. 10.2514/6.2004-1906.
[10] R. Ehrgott, H. V. Panossian, G. Davis, Modeling techniques for evaluating the effectiveness of particle damping in turbomachinery, in: AIAA/ASME/ASCE/AHS/ASC Struct. Struct. Dyn. Mater. Conf., Palm springs, California, 2009. 10.2514/6.2009-2690.
[11] Z. Lu, X. Chen, D. Zhang, K. Dai, Experimental and analytical study on the performance of particle tuned mass dampers under seismic excitation, Earthq. Eng. Struct. Dyn. 46 (2017) 697–714, https://doi.org/10.1002/eqe.2826.
[12] B.L. Fowler, E.M. Flint, S.E. Olson, Design methodology for particle damping, in: Proc. SPIE 4331, Smart Struct. Mater. 2001 Damping Isol., Newport Beach, California, 2001: pp. 186–197. 10.1117/12.432703.
[13] R.D. Friend, V.K. Kinra, Particle impact damping, J. Sound Vib. 233 (2000) 93–118, https://doi.org/10.1006/jsvi.1999.2795.
[14] Y. Wang, B. Liu, A. Tian, W. Tang, Experimental and numerical investigations on the performance of particle dampers attached to a primary structure undergoing free vibration in the horizontal and vertical directions, J. Sound Vib. 371 (2016) 35–55, https://doi.org/10.1016/j.jsv.2016.01.056.
[15] W. Liu, G.R. Tomlinson, J.A. Rongong, The dynamic characterisation of disk geometry particle dampers, J. Sound Vib. 280 (2005) 849–861, https://doi.org/10.1016/j.jsv.2003.12.047.
[16] C.X. Wong, M.C. Daniel, J.A. Rongong, Energy dissipation prediction of particle dampers, J. Sound Vib. 319 (2009) 91–118, https://doi.org/10.1016/j.jsv.2008.06.027.
[17] K. Mao, M.Y. Wang, Z. Xu, T. Chen, DEM simulation of particle damping, Powder Technol. 142 (2004) 154–165, https://doi.org/10.1016/j.powtec.2004.04.031.
[18] C. Salueña, T. Pöschel, S.E. Esipov, Dissipative properties of vibrated granular materials, Phys. Rev. E 59 (1999) 4422–4425, https://doi.org/10.1103/PhysRevE.59.4422.
[19] K. Zhang, T. Chen, L. He, Damping behaviors of granular particles in a vertically vibrated closed container, Powder Technol. 321 (2017) 173–179, https://doi.org/10.1016/j.powtec.2017.08.020.
[20] P. Eshuis, K. van der Weele, D. van der Meer, R. Bos, D. Lohse, Phase diagram of vertically shaken granular matter, Phys. Fluids 19 (2007), https://doi.org/10.1063/1.2815745.
[21] G.H. Ristow, Critical exponents for granular phase transitions, Europhys. Lett. 40 (1997) 625–630, https://doi.org/10.1209/epl/i1997-00514-3.
[22] A. Sack, M. Heckel, J.E. Kollmer, F. Zimber, T. Pöschel, Energy dissipation in driven granular matter in the absence of gravity, Phys. Rev. Lett. 111 (2013) 1–5, https://doi.org/10.1103/PhysRevLett.111.018001.
[23] N. Meyer, R. Seifried, Toward a design methodology for particle dampers by analyzing their energy dissipation, Comput. Part. Mech. (2020), https://doi.org/10.1007/s40571-020-00363-0.
[24] K. Zhang, T. Chen, X. Wang, J. Fang, Rheology behavior and optimal damping effect of granular particles in a non-obstructive particle damper, J. Sound Vib. 364 (2016) 30–43, https://doi.org/10.1016/j.jsv.2015.11.006.
[25] Z. Yin, F. Su, H. Zhang, Investigation of the energy dissipation of different rheology behaviors in a non-obstructive particle damper, Powder Technol. 321 (2017) 270–275, https://doi.org/10.1016/j.powtec.2017.07.090.
[26] P. Eshuis, K. Van Der Weele, D. Van Der Meer, D. Lohse, Granular leidenfrost effect: Experiment and theory of floating particle clusters, Phys. Rev. Lett. 95 (2005) 1–4, https://doi.org/10.1103/PhysRevLett.95.258001.
[27] T. Pöschel, T. Schwager, C. Salueña, Onset of fluidization in vertically shaken granular material, Phys. Rev. E 62 (2000) 1361–1367, https://doi.org/10.1103/PhysRevE.62.1361.
[28] C. Salueña, T. Pöschel, Convection in horizontally shaken granular material, Eur. Phys. J. E. 1 (2000) 55–59, https://doi.org/10.1007/s101890050006.
[29] N. Rivas, A.R. Thornton, S. Luding, D. Van Der Meer, From the granular Leidenfrost state to buoyancy-driven convection, Phys. Rev. E 91 (2015) 1–10, https://doi.org/10.1103/PhysRevE.91.042202.
[30] A. Sack, K. Windows-Yule, M. Heckel, D. Werner, T. Pöschel, Granular dampers in microgravity: sharp transition between modes of operation, Granul. Matter. 22 (2020) 1–6, https://doi.org/10.1007/s10035-020-01017-x.
[31] S.F. Masri, General motion of impact dampers, J. Acoust. Soc. Am. 47 (1970) 229–237, https://doi.org/10.1121/1.1911470.
[32] N. Popplewell, M. Liao, A simple design procedure for optimum impact dampers, J. Sound Vib. 146 (1991) 519–526, https://doi.org/10.1016/0022-460X(91)90707-Q.
[33] J.M. Bajkowski, B. Dyniewicz, C.I. Bajer, Damping properties of a beam with vacuum-packed granular damper, J. Sound Vib. 341 (2015) 74–85, https://doi.org/10.1016/j.jsv.2014.12.036.
[34] J.M. Bajkowski, B. Dyniewicz, M. Gębik-Wrona, J. Bajkowski, C.I. Bajer, Reduction of the vibration amplitudes of a harmonically excited sandwich beam with controllable core, Mech. Syst. Signal Process. 129 (2019) 54–69, https://doi.org/10.1016/j.ymssp.2019.04.024.
[35] K.S. Marhadi, V.K. Kinra, Particle impact damping: Effect of mass ratio, material, and shape, J. Sound Vib. 283 (2005) 433–448, https://doi.org/10.1016/j.jsv.2004.04.013.
[36] Z. Xu, M.Y. Wang, T. Chen, Particle damping for passive vibration suppression: Numerical modelling and experimental investigation, J. Sound Vib. 279 (2005) 1097–1120, https://doi.org/10.1016/j.jsv.2003.11.023.
[37] M. Saeki, Analytical study of multi-particle damping, J. Sound Vib. 281 (2005) 1133–1144, https://doi.org/10.1016/j.jsv.2004.02.034.
[38] S.E. Olson, An analytical particle damping model, J. Sound Vib. 264 (2003) 1155–1166, https://doi.org/10.1016/S0022-460X(02)01388-3.
[39] P.A. Cundall, O.D.L. Strack, A discrete numerical model for granular assemblies, Geotechnique 29 (1979) 47–65, https://doi.org/10.1680/geot.1979.29.1.47.
[40] Z. Lu, Z. Wang, S.F. Masri, X. Lu, Particle impact dampers: Past, present, and future, Struct. Control Heal. Monit. 25 (2018) 1–25, https://doi.org/10.1002/stc.2058.
[41] J.M. Boac, R.P.K. Ambrose, M.E. Casada, R.G. Maghirang, D.E. Maier, Applications of discrete element method in modeling of grain postharvest operations, Food Eng. Rev. 6 (2014) 128–149, https://doi.org/10.1007/s12393-014-9090-y.
[42] S. Bin Yeom, E. Ha, M. Kim, S.H. Jeong, S.J. Hwang, D.H. Choi, Application of the discrete element method for manufacturing process simulation in the pharmaceutical industry, Pharmaceutics 11 (2019), https://doi.org/10.3390/pharmaceutics11080414.

[43] N. Ahmad, R. Ranganath, A. Ghosal, Modeling and experimental study of a honeycomb beam filled with damping particles, J. Sound Vib. 391 (2017) 20–34, https://doi.org/10.1016/j.jsv.2016.11.011.
[44] N. Meyer, R. Seifried, Numerical and experimental investigations in the damping behavior of particle dampers attached to a vibrating structure, Comput. Struct. 238 (2020), 106281, https://doi.org/10.1016/j.compstruc.2020.106281.
[45] W.J. Stronge, Impact Mechanics, Cambridge University Press, New York, 2018.
[46] L. Vu-Quoc, X. Zhang, L. Lesburg, Normal and tangential force-displacement relations for frictional elasto-plastic contact of spheres, Int. J. Solids Struct. 38 (2001) 6455–6489, https://doi.org/10.1016/S0020-7683(01)00065-8.
[47] J. Coaplen, W.J. Stronge, B. Ravani, Work equivalent composite coefficient of restitution, Int. J. Impact Eng. 30 (2004) 581–591, https://doi.org/10.1016/j.ijimpeng.2003.10.038.
[48] A. Di Renzo, F.P. Di Maio, Comparison of contact-force models for the simulation of collisions in DEM-based granular flow codes, Chem. Eng. Sci. 59 (2004) 525–541, https://doi.org/10.1016/j.ces.2003.09.037.
[49] G. Kuwabara, K. Kono, Restitution coefficient in a collision between two spheres, Jpn. J. Appl. Phys. 26 (1987) 1219–1223, https://doi.org/10.1143/JJAP.26.1230.
[50] S. McNamara, E. Falcon, Simulations of vibrated granular medium with impact-velocity-dependent restitution coefficient, Phys. Rev. E. 71 (2005) 1–6, https://doi.org/10.1103/PhysRevE.71.031302.
[51] J.M. Lifshitz, H. Kolsky, Some experiments on anelastic rebound, J. Mech. Phys. Solids. 12 (1964) 35–43, https://doi.org/10.1016/0022-5096(64)90005-5.
[52] Y. Tsuji, T. Tanaka, T. Ishida, Lagrangian numerical simulation of plug flow of cohesionless particles in a horizontal pipe, Powder Technol. 71 (1992) 239–250, https://doi.org/10.1016/0032-5910(92)88030-L.
[53] D. Zhang, W.J. Whiten, The calculation of contact forces between particles using spring and damping models, Powder Technol. 88 (1996) 59–64, https://doi.org/10.1016/0032-5910(96)03104-X.
[54] B.K. Mishra, C.V.R. Murty, On the determination of contact parameters for realistic DEM simulations of ball mills, Powder Technol. 115 (2001) 290–297, https://doi.org/10.1016/S0032-5910(00)00347-8.
[55] H. Kruggel-Emden, E. Simsek, S. Rickelt, S. Wirtz, V. Scherer, Review and extension of normal force models for the Discrete Element Method, Powder Technol. 171 (2007) 157–173, https://doi.org/10.1016/j.powtec.2006.10.004.
[56] Altair Engineering Inc., EDEM 2021.1, (2021).
[57] H. Chen, Y.G. Xiao, Y.L. Liu, Y.S. Shi, Effect of Young's modulus on DEM results regarding transverse mixing of particles within a rotating drum, Powder Technol. 318 (2017) 507–517, https://doi.org/10.1016/j.powtec.2017.05.047.
[58] X. Fang, H. Luo, J. Tang, Investigation of granular damping in transient vibrations using Hilbert transform based technique, J. Vib. Acoust. Trans. ASME. 130 (2008), https://doi.org/10.1115/1.2827454.
[59] J.M. Bajkowski, B. Dyniewicz, C.I. Bajer, J. Bajkowski, An experimental study on granular dissipation for the vibration attenuation of skis, Proc. Inst. Mech. Eng. Part P J. Sport. Eng. Technol. 235 (2021) 13–20. 10.1177/1754337120964015.
[60] M.Y. Yang, G.A. Lesieutre, S.A. Hambric, G.H. Koopmann, Development of a design curve for particle impact dampers, in: Smart Struct. Mater. 2004 Damping Isol., Bellingham, WA, 2004: p. 450. 10.1117/12.540019.
[61] M. Masmoudi, S. Job, M.S. Abbes, I. Tawfiq, M. Haddar, Experimental and numerical investigations of dissipation mechanisms in particle dampers, Granul. Matter. 18 (2016) 1–11, https://doi.org/10.1007/s10035-016-0667-4.
[62] M.Y. Yang, Development of master design curves for particle impact dampers, The Pennsylvania State University, 2003.
[63] F. Terzioglu, J.A. Rongong, C.E. Lord, Experimental data sets of a granular damper, (2022). 10.15131/shef.data.21273282.v2.
[64] M.N. Bannerman, J.E. Kollmer, A. Sack, M. Heckel, P. Mueller, T. Pöschel, Movers and shakers: Granular damping in microgravity, Phys. Rev. E. 84 (2011) 1–9, https://doi.org/10.1103/PhysRevE.84.011301.
[65] X.Z. An, R.Y. Yang, R.P. Zou, A.B. Yu, Effect of vibration condition and inter-particle frictions on the packing of uniform spheres, Powder Technol. 188 (2008) 102–109, https://doi.org/10.1016/j.powtec.2008.04.001.
[66] B. Darabi, J.A. Rongong, Polymeric particle dampers under steady-state vertical vibrations, J. Sound Vib. 331 (2012) 3304–3316, https://doi.org/10.1016/j.jsv.2012.03.005.